# INLINE PRESSURE SENSING MECHANISMS ENABLING SCALABLE RANGE AND SENSITIVITY

*D. Alveringh[1], J. Groenesteijn[1], R.J. Wiegerink[1], and J.C. Lötters[1,2]*
[1] MESA+ Institute for Nanotechnology, University of Twente, Enschede, The Netherlands
[2] Bronkhorst High-Tech BV, Ruurlo, The Netherlands

## ABSTRACT

We report on two novel capacitive pressure sensing mechanisms that allow measurements inline with other fluidic devices on one chip, without introducing a large internal volume to the fluid path. The first sensing mechanism is based on out-of-plane bending of a U-shaped channel and the same structure could be used for thermal flow sensing simultaneously. The second mechanism is based on deformation of the cross-section of the tube and allows for differential capacitive readout. The sensitivity and range of both mechanisms are scalable. The current implementations are tested up to 2.45 bar and 1 bar respectively.

## KEYWORDS

Pressure sensor, lab-on-a-chip, surface channel technology, capacitive readout.

## INTRODUCTION

Combining fluidic sensors and actuators on one chip is interesting for various applications like flow chemistry or lab-on-a-chip devices. For example, an inline pressure sensor integrated with a valve makes pressure control possible. Or, combined flow and pressure sensors on one chip allows for viscosity measurements [1]. Most pressure sensors contain a membrane that deforms as a function of pressure, e.g. [2, 3]. These sensors are often not inline with the fluid path and introduce a dead volume, which can introduce bubbles or leave residues of previously measured fluids. Hence, there is a need for scalable inline pressure sensors that can be integrated with other devices on one chip.

## DESIGN

The two proposed sensor mechanisms are fabricated using surface channel technology [4]. This technology allows for the realization of suspended semi-circular tubes as illustrated in figure 1. The working principle of both sensors is based on pressure-induced deformation of the tube. Since both pressure sensors consist of suspended tubes, a thermal flow sensor [5] can be integrated in the same structure.

### Sensor I

Sensor I consists of a U-shaped tube. An applied pressure results in a net longitudinal force at the end of the tube (Figure 1). The difference in stiffness between the upper and lower part of the tube forces it to bend upwards. Comb-shaped electrodes convert the upward displacement in a change of capacitance.

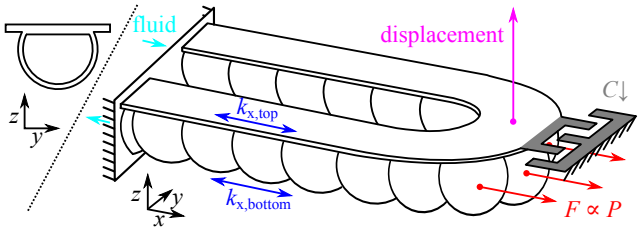


*Figure 1: Sensor I, consisting of a U-shaped tube. A pressure results in a net longitudinal force. Difference in stiffness between upper ($k_{x,top}$) and lower ($k_{x,bottom}$) part of the tube forces it to bend upwards, resulting in a change of capacitance.*

For out of plane bending, it is assumed that the semi-circular tube can be modeled as a T-beam to find the bending mechanics as shown in figure 2. One half of the U-tube is considered in the derivation of the model.

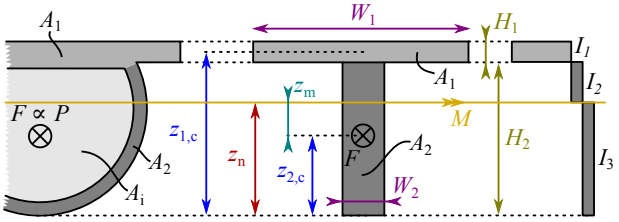


*Figure 2: The semi-circular tube modeled as a T-beam, with the dimensions, force, moment and area moments of inertia.*

A pressure $P$ results via surface area $A_i$ in a force $F$. Since the neutral axis at $z_m$ is not at the same position of the applied force, a moment can be defined:

$$M = F\, z_m = P\, A_i\, z_m. \tag{1}$$

The neutral axis passes through the center of mass of the cross section of the T-beam. The z-coordinate of the neutral axis $z_n$ can therefore be calculated using the following equation.

$$z_n = \frac{z_{1,c}\, A_1 + z_{2,c}\, A_2}{A_1 + A_2}, \tag{2}$$

with $z_{1,c}$ and $A_1$ the center and the surface area of the top part of the T-beam and $z_{2,c}$ and $A_2$ the center and the surface

area of the bottom part of the T-beam. The total area moment of inertia $I$, which is the sum of the three area moments of inertia defined in figure 2, can be expressed as follows.

$$I = \underbrace{\frac{W_1 H_1^3}{12} + A_1 \left(z_{1,c} - z_n\right)^2}_{I_1} + \underbrace{\frac{W_2 (H_2 - z_n)^3}{3}}_{I_2} + \underbrace{\frac{W_2 z_n^3}{3}}_{I_3}, \quad (3)$$

with $W_1$, $W_2$, $H_1$ and $H_2$ the dimensions as specified in figure 2. The radius of curvature $R$ of the tube can be found using:

$$\frac{1}{R} = \frac{M}{EI} \quad (4)$$

with $E$ the Young's modulus of silicon nitride. As is illustrated in figure 3, an equation for the deformation $\Delta z$ can be derived from the radius of curvature.

$$\Delta z = R - \left(R \cos\left(\frac{L_0}{R}\right)\right). \quad (5)$$

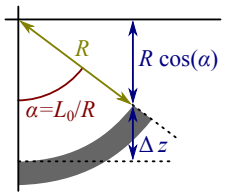


*Figure 3: The assumed circular bending of the tube with deformation $\Delta z$.*

The deformation $\Delta z$ can be measured capacitively. There is a initial offset of approximately 9 µm between the comb-structures due to residual stress. The capacitance $C$ is dependent on the deformation and is modeled using finite element simulations (COMSOL Multiphysics 4.4), see figure 4.

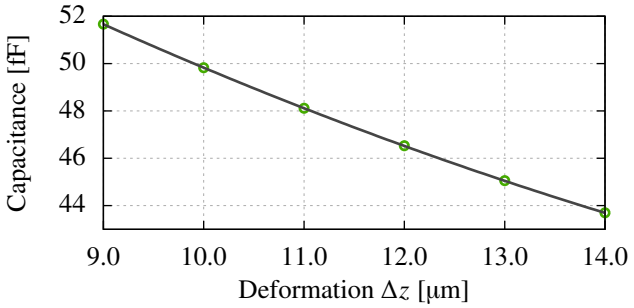


*Figure 4: Simulation results of the capacitance between the comb fingers for different displacements.*

The model including the bending mechanics and the capacitive model of Sensor I is plotted in figure 5. Since the range and sensitivity is dependent on the length of the U-tube, a prediction for multiple lengths of the tube is included in the plot.

**Sensor II**

Sensor II is based on reference [3] with additional support for inline pressure measurement and a less complicated

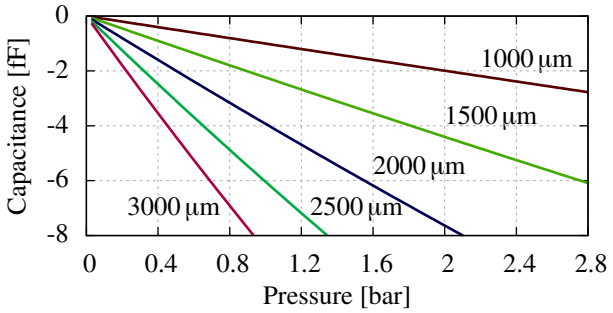


*Figure 5: Model plot of Sensor I for different tube lengths.*

fabrication process. The sensor consists of a partially released straight tube with combs on both sides. At one side, the tube has long fingers (200 µm) and the stator has short fingers (50 µm). The long fingers are slightly bent downwards due to material stress. Increase in pressure will deform the ceiling of the tube upwards, tilting the fingers downwards and increasing the distance between the fingers (Figure 6). The fingers at the other side of the tube behave vice versa, resulting in decreasing distance. This asymmetry allows differential measurement, which cancels environmental effects.

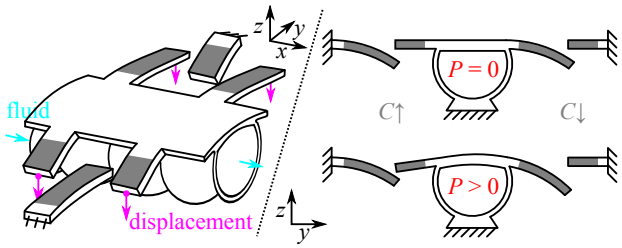


*Figure 6: Sensor II, consisting of a tube with comb-shaped electrodes. A pressure deforms the ceiling of the tube and displace the comb fingers at both sides. asymmetry of the comb finger lengths makes differential measurement possible.*

The range and sensitivity of the sensor can be changed by changing the width of the channel. A wider channel will result in a higher sensitivity, because the deformation of the tube will be higher. However, this also results in more stress and therefore limits the range. The maximum range and sensitivity are plotted in figure 7, assuming a maximum stress of 100 MPa.

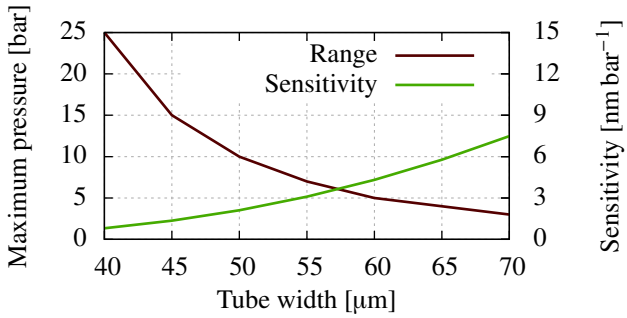


*Figure 7: Prediction of the scalability of Sensor II, based on finite element simulations.*

## FABRICATION

Fabrication of both mechanisms is based on surface channel technology [4], but also other technologies may be suitable, e.g. the polymer tube technology of [6]. SEM images of both mechanisms are shown in Figures 8 and 9 respectively. The final assembly is shown in Figure 10.

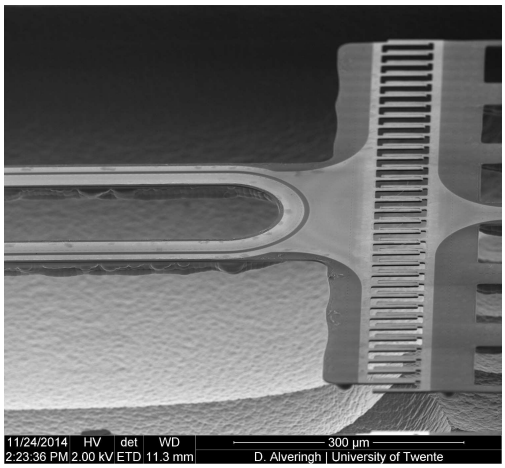


*Figure 8: SEM image of Sensor I.*

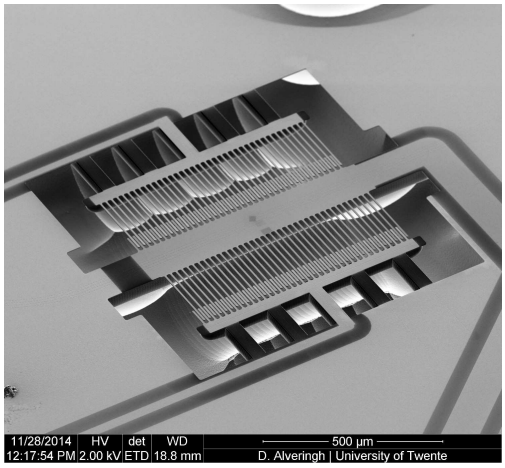


*Figure 9: SEM image of Sensor II.*

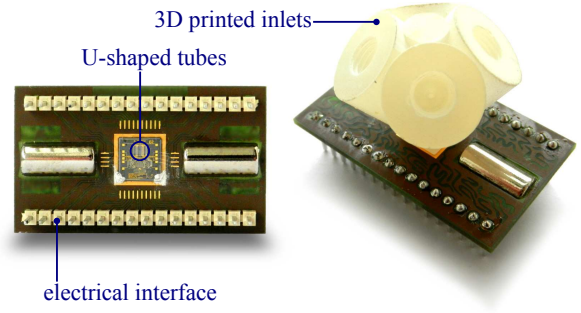


*Figure 10: Photos of the assembled chip with fluidic and electrical connections.*

## CHARACTERIZATION

The deformation and capacitance as a result of pressure are characterized for both sensors.

### Sensor I

The deformation of the tube is measured using white light interferometry (Polytec MSA-400). Figures 11 and 12 show the results.

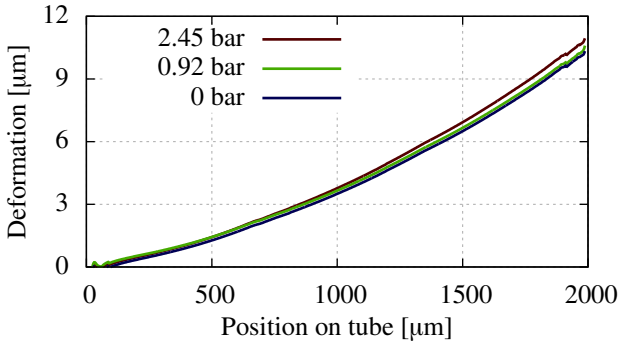


*Figure 11: Deformation of the tube for different pressures. Measured using white light interferometry.*

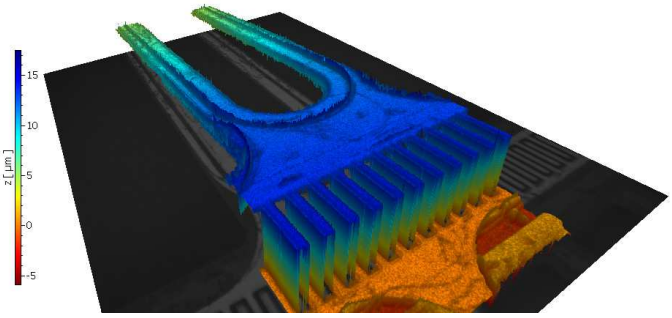


*Figure 12: White light interferometry 3D-render of the tube for a pressure of 1.84 bar.*

The capacitance is measured using a charge amplifier and a lock-in amplifier, as is illustrated in figure 13. Figure 14 shows the measurement results for an applied pressure of 0 to 2.45 bar. The solid line shows the model. It appears that the model matches the measurement results in order of magnitude. A non-linear effect occurs for higher pressures.

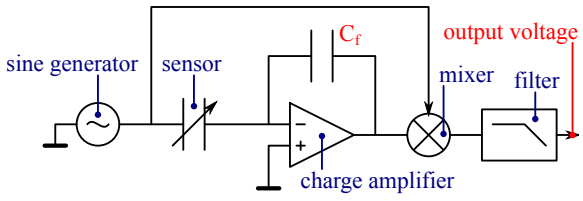


*Figure 13: Capacitive measurement setup for Sensor I.*

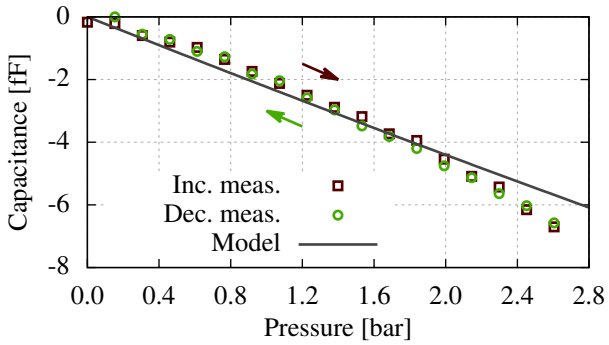


*Figure 14: Capacitive measurement results of Sensor I for increased and decreased swept pressure with model fit.*

**Sensor II**

For the differential capacitive sensing of Sensor II, sine waves of 1 MHz of opposite phase are applied to the combs on the stator (Figure 15). The signal of both capacitors is amplified using a charge amplifier and demodulated with a mixer and filter to a signal proportional to the ratio of capacitance. By controlling the amplitudes of the sine generators such that the output voltage is 0 V, the ratio of the amplitudes is equal to the ratio of the capacitances:

$$\frac{V_A}{V_B} = \frac{C_A}{C_B}. \tag{6}$$

This method enables large range measurements and completely eliminates the drift in the gain in the charge amplifier and the modulator. For short-term measurements, it is sufficient to initially tune the output voltage to 0 V and subsequently measure the output voltage as a function of pressure. Figure 16 shows the measurement results for an applied pressure of 0 to 1 bar.

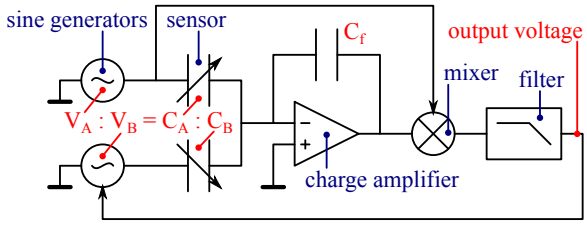


*Figure 15: Differential capacitive measurement setup for Sensor II.*

## CONCLUSION

Two inline pressure sensing mechanisms for the integration with other fluidic devices on one chip have been designed, fabricated and characterized. Sensor I has a range of 0 bar to 2.45 bar with a sensitivity of approximately 2 fF bar$^{-1}$. Sensor II has a range of 0 bar to 1 bar with a sensitivity of approximately 280 mV bar$^{-1}$. Simple redesigns of the mechanisms enable different ranges and sensitivities. Also on-tube integration of a thermal flow sensor may be possible I. A novel electronic setup is developed for differential capacitive measurements.

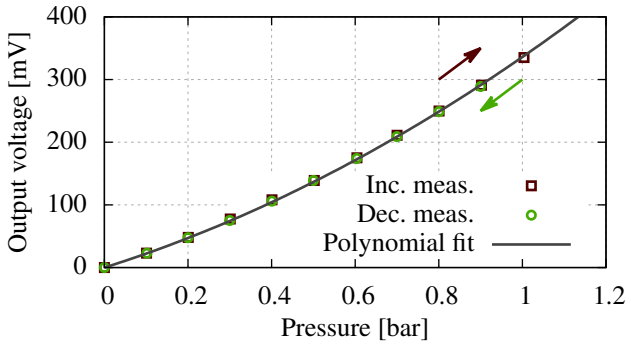


*Figure 16: Measurement results of Sensor II, with the output voltage of the setup proportional to $C_A/C_B$.*

Future work will focus on improving the modeling, enabling differential pressure measurement, integration of an on-tube flow sensor and the development of different versions with different ranges and sensitivities.

## ACKNOWLEDGEMENTS

The authors gratefully acknowledge support by the Eurostars Programme through the TIPICAL project (E!8264), NanoNextNL and Theo Lammerink for support with the measurements.

## REFERENCES

[1] J. C. Lötters *et al.*, "Integrated multi-parameter flow measurement system," in *Micro Electro Mechanical Systems (MEMS), 2014 IEEE 27th International Conference on*. IEEE, 2014, pp. 975–978.

[2] Y. Zhang *et al.*, "A high-sensitive ultra-thin mems capacitive pressure sensor," in *Solid-State Sensors, Actuators and Microsystems Conference (TRANSDUCERS), 2011 16th International*. IEEE, 2011, pp. 112–115.

[3] M. Dijkstra *et al.*, "Miniaturised Prandtl tube with integrated pressure sensors for micro-thruster plume characterisation," in *Micro Electro Mechanical Systems (MEMS), 2014 IEEE 27th International Conference on*. IEEE, 2014, pp. 999–1002.

[4] J. Haneveld *et al.*, "Modeling, design, fabrication and characterization of a micro coriolis mass flow sensor," *Journal of Micromechanics and Microengineering*, vol. 20, no. 12, p. 125001, 2010.

[5] T. S. J. Lammerink *et al.*, "Single chip flow sensing system with a dynamic flow range of more than 4 decades," in *Solid-State Sensors, Actuators and Microsystems Conference (TRANSDUCERS), 2011 16th International*. IEEE, 2011, pp. 890–893.

[6] B. Ilic *et al.*, "Fabrication of flexible polymer tubes for micro and nanofluidic applications," *Journal of Vacuum Science & Technology B*, vol. 20, no. 6, pp. 2459–2465, 2002.

**CONTACT** Dennis Alveringh - d.alveringh@utwente.nl